



Contents lists available at ScienceDirect

Biosensors and Bioelectronics

journal homepage: <http://www.elsevier.com/locate/bios>

Short communication

Real-time and noninvasive detection of UV-Induced deep tissue damage using electrical tattoos

Jae Joon Kim, Trisha L. Andrew*

Departments of Chemistry and Chemical Engineering, University of Massachusetts Amherst, Amherst, MA, 01003, United States

ARTICLE INFO

Keywords:

Bioimpedance analysis
Radiation damage
Reactive vapor deposition
Conducting polymer
Point of care sensing
Plant electronics

ABSTRACT

Understanding longterm deep tissue damage caused by UV radiation is imperative for ensuring the health and safety of living organisms that are regularly exposed to radiation sources. While existing UV dosimeters can quantify the cumulative amount of radiation to which an organism is exposed, these sensors cannot reveal the presence and extent of internal tissue damage caused by such exposure. Here we describe a method that uses conducting polymer tattoos to detect UV radiation-induced deep tissue damage in living organisms using bioimpedance analysis (BIA), which allows for noninvasive, real-time measurements of body composition and point-of-care assessment of clinical condition. To establish a performance baseline for this method, we quantify the effects of UVA radiation on live plant leaves. Low-energy UVA waves penetrate further into biological tissue, as compared to UVB, UVC and ionizing radiation, and cause longlasting deep tissue damage that cannot be immediately and readily detected using surface-sensitive techniques, such as photogrammetry and epidermal sensors. We show that single-frequency bioimpedance analysis allows for sensitive, real-time monitoring of UVA damage: as UVA dose increases, the bioimpedance of a plant leaf measured at a frequency of 1 kHz linearly decreases until the extent of radiation damage saturates and the specimen is effectively necrotized. We establish a strong correlation between radiation fluence, internal biological damage and the bioimpedance signal measured using our conducting polymer tattoos, which supports the efficacy of our method as a new type of internal biodosimetry.

1. Introduction

Radiation exposure causes immense stress and incurable damage to the exposed tissue by changing a number of structural and biochemical features in living organisms (Lerebours et al., 2018; Stone et al., 2003). Importantly, remote, real-time, sensitive monitoring of cellular stress in biological samples is crucial to detecting and preventing acute radiation damage (Blakely et al., 2005; Lacombe et al., 2018). However, in spite of increasing concerns about the health and environmental impacts of UV radiation, most radiation-detecting methods are based on surface-restricted detectors and dosimeters (Ahmadi and Yeow, 2011; Heo et al., 2018; Kim et al., 2016), which do not reveal the internal condition of living materials, such as organs, cells, and organelles. In addition, biochemical assays, though accurate, cannot be performed in the field (or at the point of care), typically call for the destructive digestion of sample tissue, and require a significant time investment that prevents real-time detection and diagnosis of radiation damage (Ferancová et al., 2010; Kudr et al., 2017).

Electrical impedance spectroscopy (EIS) and bioimpedance analysis (BIA) has been widely used in various research fields including plant biology, human physiology and food science, for noninvasive, accurate measurements of full-body composition and point-of-care assessment of clinical condition (El Khaled et al., 2018; Zhang and Willison, 1991). These methods can also quantify deep tissue damage caused by various stressors, including UV radiation (Huang et al., 2013; Osterman et al., 2004). However, use of this technique, particularly for longterm health monitoring, is limited by the composition and nature of the electrodes used to obtain a bioimpedance signal. The most widely used electrodes for bioimpedance measurements of plants are injected needles and adhesive-backed patch electrodes. However, these electrodes cause physical damage to plant specimens (Repo, 1988) and are not robust enough for longitudinal use. Further, the metal contacts in both of these electrodes either prevents or significantly attenuates UV and visible light penetration into the underlying plant tissue, which leads to erroneous data about UV damage. To combat these persistent issues, we previously reported a longlasting, vapor-deposited polymer electrode that can be

* Corresponding author.

E-mail address: tandrew@umass.edu (T.L. Andrew).<https://doi.org/10.1016/j.bios.2019.111909>

Received 10 September 2019; Received in revised form 15 November 2019; Accepted 19 November 2019

Available online 23 November 2019

0956-5663/© 2019 Elsevier B.V. All rights reserved.

directly and nondestructively applied to the surface of living organisms and used to perform bioimpedance spectroscopy (Kim et al., 2019).

Here we use our previously-reported polymer electrodes (tattoos) to detect radiation-induced deep tissue damage in living organisms using BIA. To establish a performance baseline for this method, we quantify the effects of UVA radiation on live plants by tattooing their leaves, as we identify the leaf as the part of a plant that is most exposed to and damaged by UVA radiation. Low-energy UVA waves penetrate further into biological tissue as compared to UVB, UVC and ionizing radiation, and cause longlasting deep tissue damage that cannot be immediately and readily detected using surface-sensitive techniques, such as photogrammetry and epidermal sensors. We show that single-frequency bioimpedance analysis allows for sensitive, real-time monitoring of UVA damage: as UVA dose increases, the bioimpedance of a plant leaf measured at a frequency of 1 kHz linearly decreases until the extent of radiation damage saturates and the specimen is necrotized. We also establish a strong correlation between radiation fluence, internal biological damage and the bioimpedance signal measured using our conducting polymer tattoos. Based on the promising results obtained from this model study, we propose that BIA performed using vapor-deposited polymer tattoos can be further applied to study living tissue damage caused by other radiation sources.

2. Materials and methods

2.1. Materials

Live Hosta “Pilgrim” plants were purchased from a local greenhouse in Amherst MA, United States. Prior to testing, individual leaves were cut from the plant, rinsed under running DI water, and immediately placed into a container of tap water to prevent dehydration. Materials needed for vapor deposition of the polymer tattoo, including 3,4-ethylenedioxythiophene (EDOT) and iron chloride (FeCl_3) were purchased from Sigma-Aldrich and used without any purification.

2.2. Vapor deposition of polymer tattoos

A previously-reported procedure involving a custom-built reactor (Cheng et al., 2017) was followed, with minor alterations, to deposit conducting polymer electrodes on the surface of freshly-cut Hosta leaves (Kim et al., 2019). Polymer tattoos had a high width (50 mm) to channel length (5 mm) ratio of 10:1 to achieve uniform conduction pathways during impedance measurements. A large enough channel length was used such that a sufficiently large ensemble of leaf cells would contribute to the measured impedance response. An electrode length of 20 mm was used to maximize the electrode size, which contributed to better charge injection, lower contact impedance and ease of saline droplet placement.

2.3. UV irradiation

A 300 W mercury arc lamp (Newport) was used as the radiation source. Band-pass filters were used to selectively transmit UVA (320–400 nm) light. A water-filled Petri dish was placed between the lamp and sample to prevent thermal damage during irradiation and further absorb stray UVB and UVC light. The intensity of UVA light reaching the sample surface was quantified using a UV power meter (OAI 306) and compared with the intensity of UVA radiation contained in sunlight in Table S1. The highest sunlight intensities were measured on a sunny day at 1 p.m. August in Amherst, Massachusetts, United States, latitude 42.3°. UVA fluence values were calculated for two wavelengths, 365 nm and 400 nm, by measuring the light output intensities of the lamp at these wavelengths using a UV power meter and using Equation (1):

$$\text{UVA Fluence} = \frac{N}{A} = \frac{E_N}{E_1} \times \frac{1}{A} = I_N t \times \frac{\lambda}{hc} \quad (1)$$

Here, N is the number of photons of wavelength λ , A is the area of the sample that was exposed to irradiation, E_N is the energy of N photons of wavelength λ , E_1 is the energy of one photon of wavelength λ , I_N is the measured light output intensity at wavelength λ , h is Planck’s constant, c is the speed of light, and λ is the wavelength of interest. Calculated fluence values at 365 nm and 400 nm were then averaged to obtain the “UVA Fluence” values used throughout this work.

2.4. Bioimpedance measurements

Bioimpedance spectroscopy was performed with an impedance analyzer (Agilent 4294A). A low drive voltage of 100 mV was applied to prevent electrochemical side reactions. Impedance was measured over the frequency range of 100 Hz to 1 MHz. To exclude impedance contributions from varying electrical contact across different leaf samples, a droplet of 1M saline solution was placed on the polymer electrode surface and the probe tips of the impedance analyzer inserted into this droplet. The saline droplet was automatically and selectively confined over the hydrophilic polymer electrode and was not observed to spread onto other areas of the Hosta leaf surface. Data fitting and equivalent circuit modelling were performed using ZView2 software (Princeton Applied Research). Linear fits were obtained using Origin Pro2016 (Origin) software.

3. Results and discussion

3.1. Vapor-deposited conducting polymer electrodes on a plant leaf

To measure and monitor radiation damage of tissue using bioimpedance analysis, we created patterned conducting polymer electrodes (tattoos) on plant leaves using reactive vapor deposition (Fig. 1). The plant used in this study was Hosta, a widely-used landscape plant whose leaves are particularly susceptible to photolytic damage (Fig. S1). Freshly cut Hosta leaves were placed into a custom-built reactor after tape masking to be coated with the polymer tattoos, then subsequently rinsed to remove residual iron salts. During the vapor deposition process, a persistently p-doped conducting polymer, PEDOT-Cl, was created inside the reactor and directly on the surface of the Hosta leaf. Similar to our previous report,⁶ the surface conductivity of the vapor deposited polymer tattoo thus obtained was 1 S/cm. As seen in Fig. 1, tattooed Hosta leaves displayed similar liveness and leaf color as their pristine counterparts, indicating that the vapor deposition process did not perturb the starting chlorophyll and water content of the leaf. Scanning electron micrographs of a polymer tattoo revealed crisp edges and an identical surface morphology as uncoated areas.

3.2. UV irradiation of plant leaves

For this model study, we chose to quantify the effects of UVA radiation on Hosta leaves. Low-energy UVA waves (320–400 nm) penetrate further into biological tissue as compared to UVB, UVC and ionization radiation (Barolet, 2008), and cause longlasting deep tissue damage resulting from the creation of reactive oxygen species (similar to other sources of ionizing radiation) (Giannakis et al., 2016; Scharffetter et al., 1991). Further, reliable and steady doses of UVA radiation could be economically obtained in a laboratory setting.

The lamp setup used to irradiate plants samples is shown in Fig. 2. A water-filled Petri dish was used as an infrared filter to prevent thermal damage to Hosta leaf samples during irradiation. This water filter also served to absorb stray UVB and UVC light (Boer et al., 1982; Smith and Baker, 1981). The output intensity of UVA light from this laboratory setup was compared to that of sunlight in Table S1. The measured lamp UVA outputs of 16.01 and 25.03 mW cm^{-2} at 365 and 400 nm,

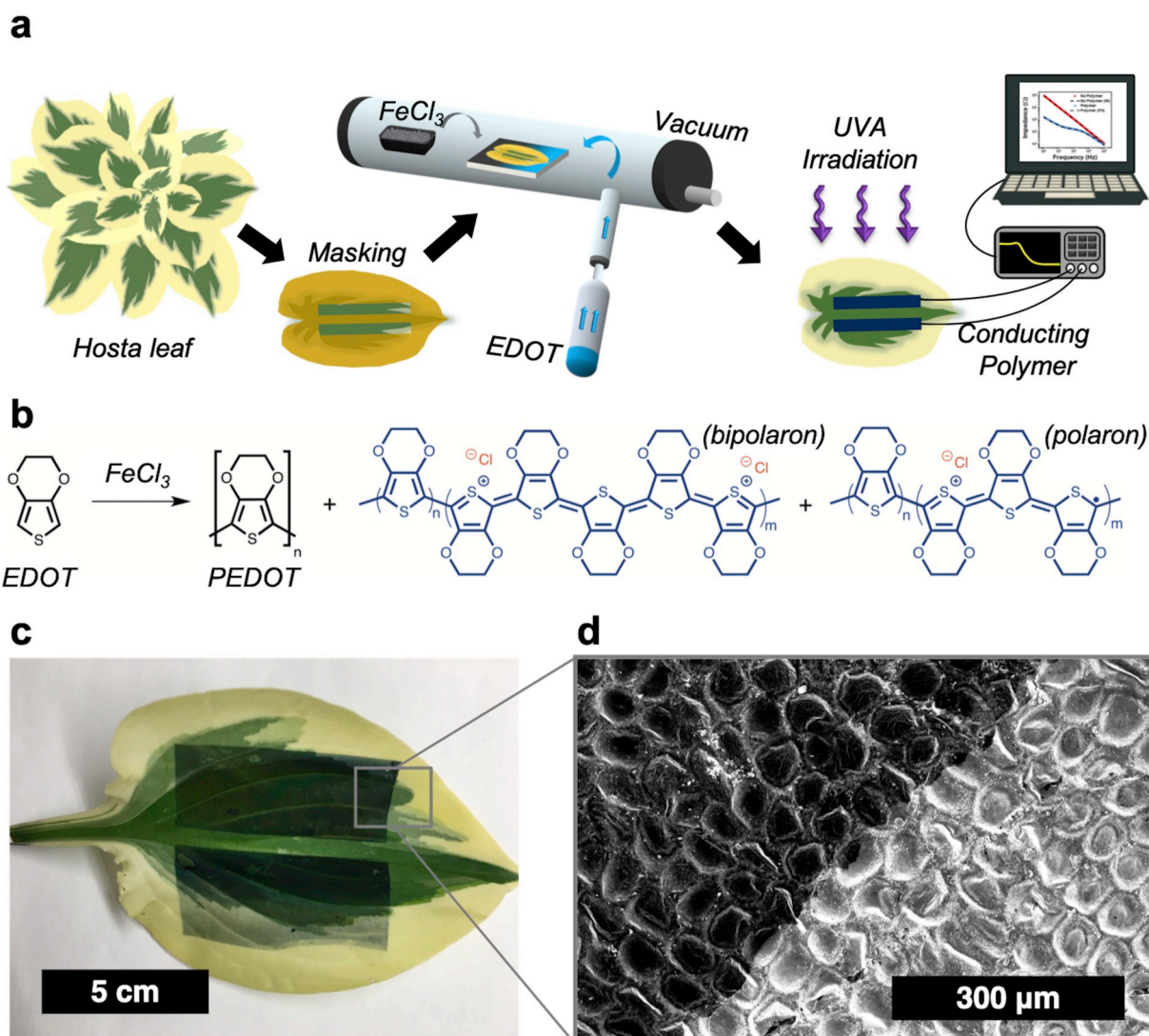


Fig. 1. (a) Summary scheme of using vapor deposited polymer tattoos to detect UVA induced tissue damage in Hosta leaves with bioimpedance analysis. (b) Polymerization reaction and structure of the conducting polymer formed on the leaf surface during vapor deposition. (c) Image of a Hosta leaf decorated with polymer tattoos. (d) A scanning electron micrograph (SEM) showing a polymer coated (top left) and pristine (right bottom) leaf surface.

respectively, were 5–6 times higher than those found in sunlight. UVA damaged leaf tissue was visibly bleached to a yellow-white color and the damaged areas were observed to be rougher than masked (UV-protected) regions (Fig. 2c). These changes were attributed to destruction of leaf chlorophyll content and cell damage, similar to what was observed in sun-damaged Hosta plants (Fig. S1). A similar protective effect was achieved by using thick (1 μm) polymer tattoo. As experimentally confirmed in Fig. S2 and supported by previous work (Lin et al., 2007), the conductivity of PEDOT-Cl did not change appreciably after 6 h of irradiation, confirming that our polymer tattoos could be reliably used for longterm monitoring of radiation damage with minimal concerns about their chemical and electrical stability.

Optical micrographs of pristine and UVA-damaged leaves revealed that the fluid-filled vacuoles of each cell (seen as white/bright circles in the images) were severely shrunken in the UVA-damaged sample. Additionally, the void area between cells was noticeably larger in the UVA-damaged sample as a result of widespread structural collapse. Fig. 2f depicts the simplified cell structure of a pristine Hosta leaf, and Fig. 2g summarizes the changes resulting from UVA exposure.

3.3. Bioimpedance spectroscopy

All organisms are composed of a mixture of ionically conductive electrolytes (interstitial fluids and intracellular fluids) and insulating structural components (membranes). When a sinusoidally varying voltage is applied through two conducting polymer tattoos, a current passes through all available cells and interstitial spaces within the sample tissue (Zhang and Willison, 1991). To understand this current, first we reduce each cell to a simple equivalent circuit composed of resistors and capacitors (Ando et al., 2017; Zhang et al., 1995). The impedance can be expressed by the resistor-like fluids (extracellular fluid, cytoplasm and vacuole sap) divided by the capacitor-like components (cell membrane, tonoplast). Depending on the frequency of the applied voltage, each component is defined as described in Note S1.

For polydisperse ensembles of cells, such as those found throughout a plant leaf, the capacitance is typically substituted by a constant phase element (CPE) as defined in Note S2. A CPE better represents the chemical and structural dispersity of the numerous kinds of cells that are present in a whole leaf (Ando et al., 2014). Resistor-like regions display frequency-independent impedance and zero-degree phase. Capacitor-like regions display a linear decrease in impedance and a decrease of the phase towards -90° .

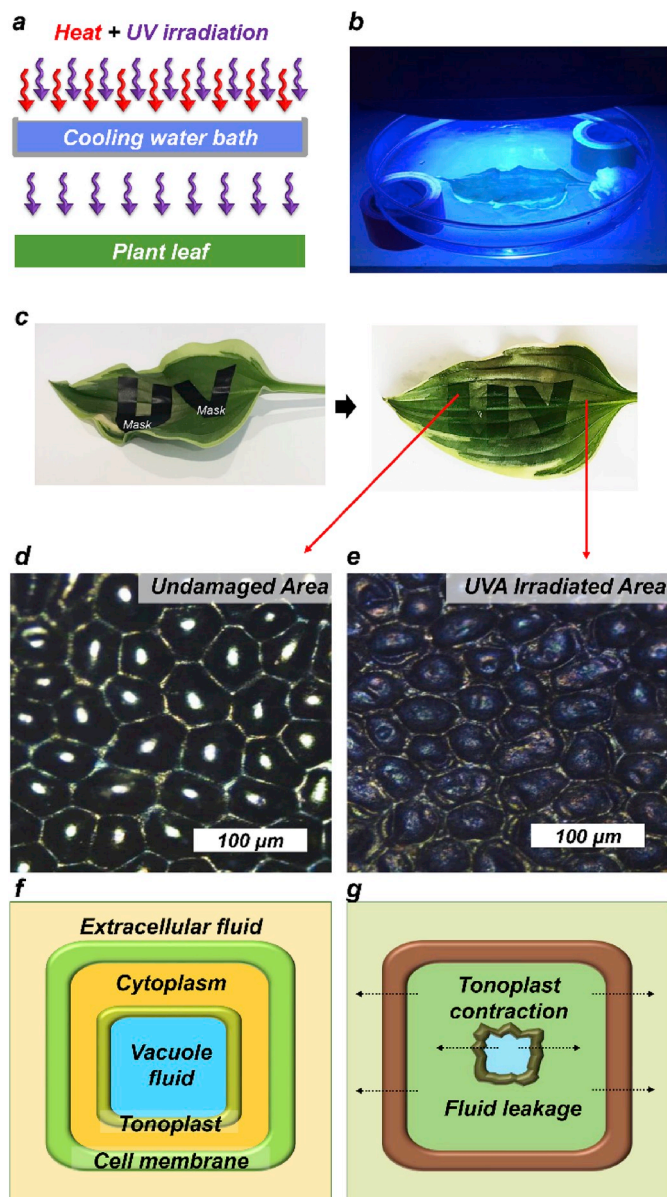


Fig. 2. (a) Scheme and (b) photograph of the setup used to irradiate samples with UVA. (c) Patterned Hosta leaf irradiated with “UV” shaped tape mask. Optical micrographs of (d) a pristine hosta leaf and (e) the same leaf after 6 h of UVA exposure. Cartoon of (f) a Hosta leaf cell and (g) a UVA irradiated cell.

The process of estimating an equivalent circuit begins by taking an inventory of the cell components that are unique to each specimen. Hosta leaf cells contain a cell membrane, extracellular fluid, cytoplasm, a vacuole and vacuole sap, and a tonoplast membrane. Some of these components can be seen in the optical micrograph image in Fig. 2d. The accepted equivalent circuit model for a Hosta leaf, which includes all these components, is called a modified double shell model (Fig. S3, Note S2) (Zhang and Willison, 1992; Zhang et al., 1993).

The Bode plot of impedance vs. frequency for a Hosta leaf decorated with electrical tattoos is shown in Fig. S4. The capacitor-like behavior between $10^3 - 10^6$ Hz is called the beta dispersion and originates from the polarization response of capacitor components (Gersing, 1998). As expected from the accepted circuit model for Hosta leaves, the Bode plot clearly shows two beta dispersions centered at 10^3 and 10^5 Hz, corresponding to the cell membrane and tonoplast, respectively.

3.4. Bioimpedance spectroscopy of UVA damages leaves

Fig. 3 displays the successive change in impedance with accumulating UVA damage on the same Hosta leaf. As the fluence of UVA radiation increased, both impedance and phase responses for the same leaf changed across all frequency ranges. A global decrease in impedance was manifested with increasing UVA exposure, with major attenuations observed at 10^3 and 10^5 Hz (Fig. S5). In particular, a near-complete loss of the beta dispersion originating from the tonoplast capacitance at 10^5 Hz was observed after 6 h of continuous UVA exposure, indicating destruction of the tonoplast. This observation was consistent with the UVA-induced vacuole damage seen in the optical micrograph image in Fig. 2e. Tonoplast damage likely arises upon UVA exposure due to creation of reactive oxygen species within the vacuole sap, which slowly degrade the long-chain fatty acids that comprise the tonoplast membrane.

Interestingly, the external cell membranes, which give rise to the beta dispersion at 10^3 Hz, degraded comparatively slower with UVA exposure. Such retarded degradation rates can be attributed to differences in the molecular composition of the cell membrane versus the tonoplast and, also, the presence of ion channels in the cell membrane that can potentially act as vents to expel reactive oxygen species before they can cause chemical damage (BAIER et al., 1990; Flowers and Yeo, 1992).

Nyquist plots (Fig. S6) provide further insight into the cell structure damage caused by UVA radiation. Both the real and imaginary parts of the impedance response decreased with UVA exposure, and a semi-circular component became more prominent with increasing degrees of damage. A semicircle in the Nyquist plot arises due to significant concentrations of ionic species. As the tonoplast membrane degrades with UVA radiation, the ion-rich vacuole sap is emptied into the cytoplasm and extracellular fluid, which should increase the overall ionic conductivity of the leaf. Further, reactive oxygen species create charged byproducts upon reacting with various cell and membrane components, which should also lead to increased ionic conductivity throughout the sample.

We also confirmed that the observed changes in the impedance response of the UVA irradiated Hosta leaf did not arise due to natural aging. Fig. 3b shows the impedance response of a freshly-cut Hosta leaf

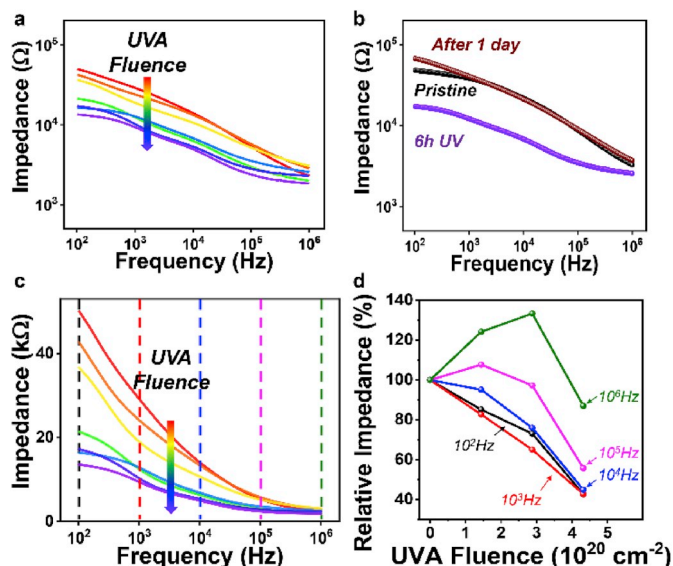


Fig. 3. (a) The impedance vs. frequency plot of a Hosta leaf with increasing UVA exposure. (b) A comparison of the impedance signal for an aged leaf versus a UVA irradiated leaf. (c) The impedance vs. frequency response plotted on a log-linear axis. The dotted lines correspond to a single frequency. (d) Impedance vs. UVA fluence at various applied voltage frequencies.

decorated with polymer tattoos and the impedance response of this same leaf after it was placed in room temperature water for 24 h. No changes were observed in the overall impedance response of the leaf after 24 h of aging, particularly the beta dispersions at 10^3 and 10^5 Hz. In contrast, these beta dispersions were nearly eradicated after the day-old leaf was exposed to UVA radiation for 6 h. Therefore, we reasonably concluded that we could specifically detect UVA damage in plants using bioimpedance spectroscopy, even if sample is naturally aging.

3.5. Dosimetry of UVA damage using bioimpedance analysis (BIA)

Although bioimpedance spectroscopy coupled with circuit modelling and fitting can reveal detailed information about the body composition and health status of living organisms, a full-frequency-sweep analysis (such as that described in the section above) requires bulky equipment and significant processing power, which are best suited for stationary lab settings. To overcome this limitation, single-frequency bioimpedance analysis (BIA) can be used for portable measurement of the health effects of specific stressors. In BIA, the raw impedance or phase output of a sample is measured at a single, carefully-identified voltage frequency and correlated, without further data processing, to the concentration of a specific stressor based on a well-developed calibration curve. This process allows for real-time, point-of-care diagnosis and the use of reasonably lightweight, hand-held equipment (Jaffrin and Morel, 2008; Karelis et al., 2013).

To enable reliable and portable detection and dosimetry of deep tissue damage induced by UVA exposure, we quantified UVA damage in *Hosta* leaves using bioimpedance analysis. Upon replotting the data shown in Fig. 3a on a log-linear axis (Fig. 3c), we observed that the measured impedance at selected frequencies linearly decreased with accumulated UVA exposure, up to 3 h (UVA fluence = 4.32×10^{20} cm⁻²). Tissue damage was saturated and samples were effectively necrotized past 3 h of UVA irradiation in our lab setup and, therefore, impedance signals past 3 h remained low and mostly unchanging (Fig. S7). Plotting the measured impedance at selected frequencies versus UVA fluence (Fig. 3d) allowed us to perform linear regression analysis to identify the most suitable voltage frequency for BIA of UVA damage. Values from the linear regression analysis of measured impedance versus fluence for five different applied voltage frequencies are tabulated in Table S2. Impedance values measured at an applied frequency of 10^3 Hz (where the signal arising from the cell membrane capacitance was located), displayed the greatest linearity, with an adjusted r-square value of 0.99, and standard deviation of 1.57% and 0.84% for the intercept and slope, respectively (Note S3). Such high linearity confirmed a strong correlation between UVA fluence and the bioimpedance output measured at 10^3 Hz, as compared to other frequencies. The calibration equation (Equation (2)) obtained via linear regression analysis for translating bioimpedance signal to UVA fluence is as follows:

$$Z_t(\%) = -18.94t + 101.04 = \frac{1.32 \times 10^{-19}}{\text{UVA Fluence}} + 101.04 \quad (2)$$

Here, Z_t is the impedance after certain time (hour), t is the irradiation time (hour) and the UVA Fluence was calculated using Equation (1).

By monitoring the change of bioimpedance at 10^3 Hz and using the equation above, we can quantify the equivalent fluence of UVA radiation to which a living sample has been exposed. In addition, the multicellular, ensemble nature of bioimpedance analysis further increases the reliability of our approach. While the median diameter of a cell is 50 μ m, the width of one tattoo electrode is 50 mm and the in-plane inter-electrode spacing is 5 mm, meaning that the output of a measurement will always be the average impedance of at least 10^5 cells, likely more. This inherently large sampling size elevates our method from other known dosimeters and ensures reliable and accurate damage prediction, even when other stress factors are present.

4. Conclusions

In summary, we used a noninvasive and rugged polymer tattoo that is applied onto the unmodified outer surface of living organisms to detect deep tissue damage induced by UVA radiation. Our unique vapor coating method enabled the conformal and damage-free preparation of conductive tattoos directly on living plant surfaces. A bioimpedance signal for live *Hosta* leaves could be readily measured using two tattoos as electrodes. We showed that single-frequency bioimpedance analysis allowed for sensitive, real-time monitoring of UVA damage in *Hosta* leaves: as UVA dose increased, the bioimpedance of a plant leaf measured at a frequency of 1 kHz linearly decreased until the extent of radiation damage saturated and the specimen was effectively necrotized. We established a strong correlation between radiation fluence, internal biological damage and the bioimpedance signal measured using our conducting polymer tattoos, which supported the efficacy of our method as a new type of internal biodosimetry.

Based on the generality, simplicity, biocompatibility and nondestructive nature of the method described herein, we expect that bioimpedance analysis performed with vapor-deposited polymer tattoos can be extended to develop portable dosimeters for detection of deep tissue damage caused by exposure to other forms of high-energy and/or ionizing radiation. We anticipate that our approach can be broadly applied to monitor radiation damage in agriculture, environmental engineering, radiotherapy, medical imaging, and biotechnology.

Declaration of competing interest

The authors declare that they have no known competing financial interests or personal relationships that could have appeared to influence the work reported in this paper.

CRediT authorship contribution statement

Jae Joon Kim: Conceptualization, Data curation, Formal analysis, Investigation, Methodology, Resources, Writing - original draft. **Trisha L. Andrew:** Conceptualization, Funding acquisition, Project administration, Resources, Supervision, Writing - original draft.

Acknowledgements

This material is based upon work supported by the National Science Foundation (USA) under CHEM MSN 1807743. J.J.K. gratefully acknowledges support from the Nuclear Global Postdoc Fellowship Program provided by the Korea Nuclear International Cooperation Foundation (KONICOF). We thank M. Formosi from the Durfee Conservatory at the University of Massachusetts Amherst for providing a wide variety of plant leaf and flower samples.

Appendix A. Supplementary data

Supplementary data to this article can be found online at <https://doi.org/10.1016/j.bios.2019.111909>.

References

- Ahmadi, M., Yeow, J.T.W., 2011. *Biosens. Bioelectron.* 26 (5), 2171–2176.
- Ando, Y., Hagiwara, S., Nabetani, H., 2017. *J. Food Eng.* 199, 9–18.
- Ando, Y., Mizutani, K., Wakatsuki, N., 2014. *J. Food Eng.* 121, 24–31.
- BAIER, M., GIMMLER, H., HARTUNG, W., 1990. *J. Exp. Bot.* 41 (3), 351–358.
- Barolet, D., 2008. Light-emitting diodes (LEDs) in dermatology. *Semin. Cutan. Med. Surg.* 227–238. No longer published by Elsevier.
- Blakely, W.F., Salter, C.A., Prasanna, P.G., 2005. *Health Phys.* 89 (5), 494–504.
- Boer, J., Schothorst, A., Boom, B., Hermans, J., Suurmond, D., 1982. *Arch. Dermatol. Res.* 273 (3–4), 247–259.
- Cheng, N., Zhang, L., Kim, J.J., Andrew, T.L., 2017. *J. Mater. Chem. C* 5 (23), 5787–5796.
- El Khaled, D., Novas, N., Gazquez, J.-A., Manzano-Agugliaro, F., 2018. *Publications* 6 (1), 6.

- Ferancová, A., Rengaraj, S., Kim, Y., Labuda, J., Sillanpää, M., 2010. *Biosens. Bioelectron.* 26 (2), 314–320.
- Flowers, T.J., Yeo, A.R., 1992. *Ion Transport across the Plasma Membrane and Tonoplast. Solute Transport in Plants*. Springer Netherlands, Dordrecht, pp. 48–73.
- Gersing, E., 1998. *Bioelectrochem. Bioenerg.* 45 (2), 145–149.
- Giannakis, S., López, M.I.P., Spuhler, D., Pérez, J.A.S., Ibáñez, P.F., Pulgarin, C., 2016. *Appl. Catal., B* 199, 199–223.
- Heo, S.Y., Kim, J., Gutruf, P., Banks, A., Wei, P., Pielak, R., Balooch, G., Shi, Y., Araki, H., Rollo, D., Gaede, C., Patel, M., Kwak, J.W., Peña-Alcántara, A.E., Lee, K.-T., Yun, Y., Robinson, J.K., Xu, S., Rogers, J.A., 2018. *Sci. Transl. Med.* 10 (470), eaau1643.
- Huang, Y.-J., Huang, E.-Y., Cheng, K.-S., 2013. *Biomed. Eng. Online* 12 (1), 23.
- Jaffrin, M.Y., Morel, H., 2008. *Med. Eng. Phys.* 30 (10), 1257–1269.
- Karelis, A.D., Chamberland, G., Aubertin-Leheudre, M., Duval, C., 2013. *Appl. Physiol. Nutr. Metabol.* 38 (1), 27–32.
- Kim, J.J., Allison, L.K., Andrew, T.L., 2019. *Sci. Adv.* 5 (3) eaaw0463.
- Kim, J.J., Ha, J.M., Lee, H.M., Raza, H.S., Park, J.W., Cho, S.O., 2016. *ACS Appl. Mater. Interfaces* 8 (30), 19192–19196.
- Kudr, J., Richtera, L., Xhaxhiu, K., Hynek, D., Heger, Z., Zitka, O., Adam, V., 2017. *Biosens. Bioelectron.* 92, 133–139.
- Lacombe, J., Sima, C., Amundson, S.A., Zenhausern, F., 2018. *PLoS One* 13 (6), e0198851.
- Lerebours, A., Gudkov, D., Nagorskaya, L., Kaglyan, A., Rizewski, V., Leshchenko, A., Bailey, E.H., Bakir, A., Ovsyanikova, S., Laptev, G., 2018. *Environ. Sci. Technol.* 52 (16), 9442–9450.
- Lin, Y.-J., Yang, F.-M., Huang, C.-Y., Chou, W.-Y., Chang, J., Lien, Y.-C., 2007. *Appl. Phys. Lett.* 91 (9), 092127.
- Osterman, K.S., Hoopes, P.J., DeLorenzo, C., Gladstone, D.J., Paulsen, K.D., 2004. *Phys. Med. Biol.* 49 (5), 665.
- Repo, T., 1988. *Physical and physiological aspects of impedance measurements in plants. Silva Fennica* 22 (3), 5351. <https://doi.org/10.14214/sf.a15508>.
- Scharffetter, K., Wlaschek, M., Hogg, A., Bolsen, K., Schothorst, A., Goerz, G., Krieg, T., Plewig, G., 1991. *Arch. Dermatol. Res.* 283 (8), 506–511.
- Smith, R.C., Baker, K.S., 1981. *Appl. Opt.* 20 (2), 177–184.
- Stone, H.B., Coleman, C.N., Anscher, M.S., McBride, W.H., 2003. *Lancet Oncol.* 4 (9), 529–536.
- Zhang, M., Willison, J., 1991. *J. Exp. Bot.* 42 (11), 1465–1475.
- Zhang, M.I.N., Repo, T., Willison, J.H.M., Sutinen, S., 1995. *Eur. Biophys. J.* 24 (2), 99–106.
- Zhang, M.I.N., Willison, J.H.M., 1992. *Can. J. Plant Sci.* 72 (2), 545–553.
- Zhang, M.I.N., Willison, J.H.M., Cox, M.A., Hall, S.A., 1993. *Can. J. Bot.* 71 (12), 1605–1611.